Mirnov coil-based plasma state classification with deep learning methods.

Hyeongjun Noh, Chweeho Heo, Yong-Su Na*

Seoul National University, Department of Nuclear Engineering, Seoul, Republic of Korea

1. Introduction

Tokamak plasmas are typically distinguished into two primary confinement modes: L-mode and H-mode, distinguished by the presence of an Edge Transport Barrier (ETB). H-mode has been adopted as the baseline operational scenario for the ITER [1] due to its enhanced confinement properties. Accurate classification of these modes is critical for stable tokamak operation and plasma control, particularly to predict disruptions like those caused by the Greenwald density limit, which show H-to-L back transition precursors [2]. Identifying these precursors via plasma state classification enables early warning systems, emphasizing the need for mode classification.

Plasma state classification has been studied using supervised deep learning (DL) methods with diagnostics like line-averaged density ($\bar{n}_e$), D_α emission, plasma current (I_p), and Mirnov Coil signals (MC) [3-9]. However, human-labelled data introduces errors and limits temporal resolution. In future DEMO reactors, high-energy neutron fluxes may impair diagnostics, requiring methods with minimal diagnostic reliance. This study proposes an unsupervised DL framework using only MC signals, planned for DEMO plasma control [10]. An autoencoder compresses MC data into a latent vector, processed via Uniform Manifold Approximation and Projection (UMAP) [12], achieving L- and H-mode classification comparable to existing methods without human intervention.

2. Methods

An autoencoder-based DL model compresses MC signals from the KSTAR tokamak into latent vectors capturing essential plasma state information. These vectors are processed using the UMAP dimensionality reduction algorithm to classify L-mode and H-mode plasma states.

2-1. Mirnov Coil Data from KSTAR

MC signals from KSTAR, measuring edge magnetic fluctuations (dB/dt) at 2 MHz in toroidal and poloidal arrays, are used to classify confinement modes. For simplicity, this research employs signals from channels 14 and 16 of the toroidal array. The signals are downsampled by a factor of four and processed via Fast Fourier Transform (FFT). For MC signal $\frac{\mathrm{d}B_i(t)}{\mathrm{d}t}$ from i-th channel, the complex Fourier transform is denoted as $X_i(f)$. Cross power is defined as $P = \left|X_i X_j^\dagger\right|$ and cross phase is defined as $\delta = \tan^{-1}\left(\frac{\mathrm{Im}(X_i X_j^\dagger)}{\mathrm{Re}(X_i X_j^\dagger)}\right)$, where $X_j^\dagger$ is the complex conjugate of j-th channel's Fourier transform, and Re and Im denote the real and imaginary parts,

respectively. Data from 7,665 KSTAR shots (2017–2022) yielded 1,241,538 chunks.

2-2. Optimal Autoencoder System for Instability Study

The Optimal Autoencoder System for Instability Study (OASIS) is an autoencoder that processes 50 ms chunks of cross power and cross phase data. The encoder compresses these inputs into latent vectors, compressing about 100-times, while the decoder reconstructs original inputs from these latent vectors, confirming the vectors capture plasma state information. To enhance performance, the encoder uses a path aggregation network (PAN) [13], which, unlike conventional CNNs that rely on high-level features, integrates features across all levels. Originally developed for image segmentation to handle varying object scales, PAN effectively captures both low- and high-frequency mode information in the latent vector.

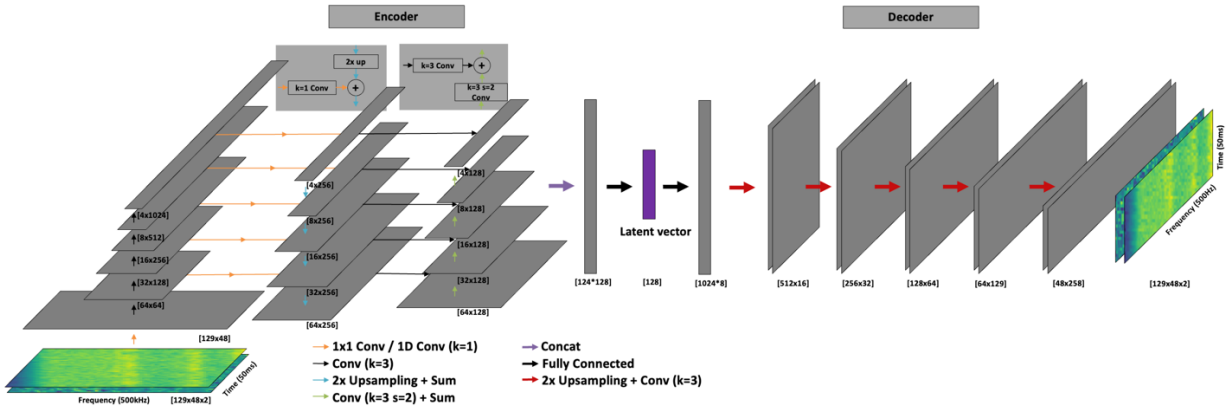

Figure 1. OASIS model architecture.

2-3. Clustering Latent Vectors to Classify Plasma States

The UMAP algorithm processes the 128-dimensional latent vectors from the OASIS autoencoder into a three-dimensional representation for visualisation. This maintains structural integrity while clustering similar plasma states. As shown in Fig. 3, L- and H-modes are distinctly separated using a threshold of 2.5 on the first UMAP axis.

Results

3-1. Reconstruction Performance of OASIS

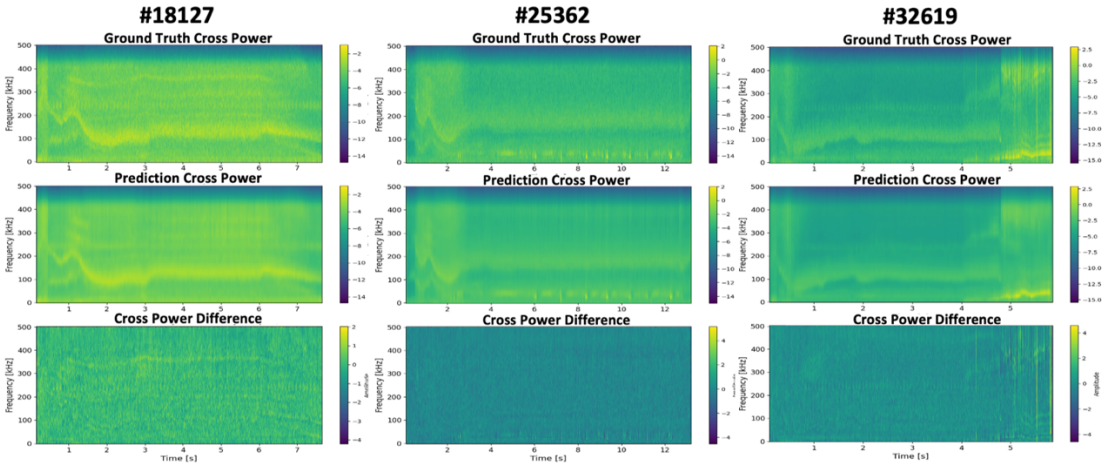

Figure 2. Three random test cases of OASIS from independent test dataset.

The performance of the OASIS model is evaluated by comparing reconstructed outputs with ground truth data. As illustrated in Fig. 2, three test cases demonstrate that the predicted reconstructions closely match the ground truth, with consistent MHD mode signals observed in both. The difference between ground truth and predictions exhibits only minimal noise without structured patterns, indicating robust model performance. To assess the effectiveness of the PAN structure in the encoder, a performance comparison was conducted with a conventional CNN-based autoencoder. As reported in Table 1, the OASIS model with PAN encoder outperforms the CNN-based model across MSE, SSIM and PSNR, where these metrices are defined as:

Mean Squared Error, $\mathrm{MSE} = \frac{1}{NM}\sum_{i=1}^{M}\sum_{j=1}^{N}\big(I(i,j) - K(i,j)\big)^2$, measures the average squared difference between reconstructed and original signals. Here, $I(i,j)$ is the original image pixel, $K(i,j)$ is reconstructed image pixel and N, M are the image size. **Structural Similarity Index,** $SSIM(x,y) = \frac{(2\mu_x\mu_y+C_1)(2\sigma_{xy}+C_2)}{(\mu_x^2+\mu_y^2+C_1)(\sigma_x^2+\sigma_y^2+C_2)}$, evaluates the similarity in luminance, contrast, and structure between them. Here, μ_x and μ_y are the means, σ_x^2 and σ_y^2 are the variances, σ_{xy} is the covariance of the original and reconstructed signals, and C_1 and C_2 are constants to stabilise the division.

Peak Signal-to-Noise Ratio, $\mathrm{PSNR} = 10 \cdot \log_{10}\left(\frac{L^2}{\mathrm{MSE}}\right)$, is the ratio of the maximum signal power to the noise in the reconstruction. Here, L is the maximum possible signal value, and MSE is the mean squared error.

Encoder Model	Decoder Model	MSE(↓)	SSIM(↑)	PSNR(↑)
PAN	**CNN**	**0.298**	**0.670**	**18.66**
PAN	PAN	0.336	0.663	17.96
CNN	CNN	2.471	0.571	9.36

Table 1. Model comparison

3-2. Results of Plasma State Classification

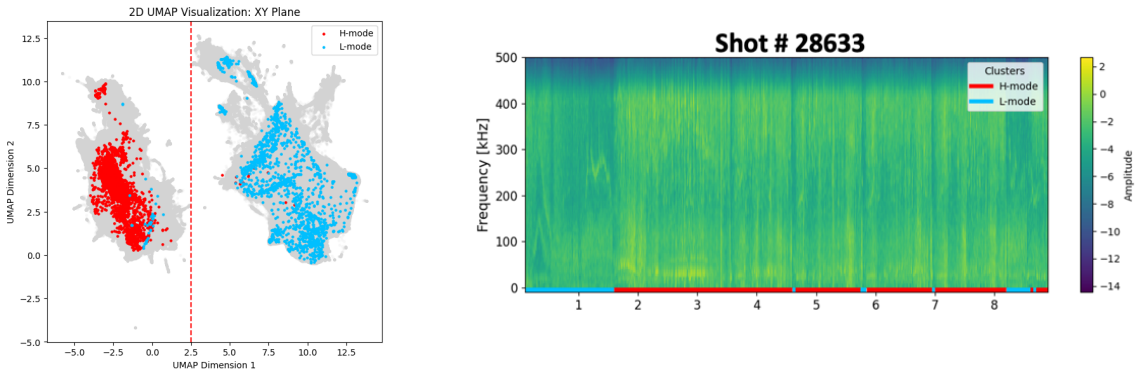

Figure 3. (Left) L- H- mode label on UMAP projection. (Right) Mode classification result of KSTAR # 28633.

The plasma state classification performance was evaluated using human-labelled data from 40 shots conducted in 2021, sourced from [8]. The model achieved 98.9% accuracy, correctly predicting 4,941 out of 4,995 test cases.

Furthermore, as shown in Fig. 3, analysis of shot 28633 reveals that the model correctly identified three out of four intermittent H-L back transitions induced by impurity seeding. The missed transition is likely due to its duration being shorter than the 50 ms chunk length used in the OASIS framework. Future work will investigate reducing the chunk length to 1–2 ms to determine if this enhances the detection of such back transitions.

Conclusion

The OASIS autoencoder compressed KSTAR MC data into a latent space, which was visualised in 3D using UMAP, achieving 98.9% accuracy in distinguishing L- and H-modes. This unsupervised approach, without labelled data, effectively identified both L-H transitions and H-L back transitions, demonstrating robust plasma state classification for tokamak control.

Acknowledgement

This research was supported by the MSIT(Ministry of Science, ICT), Korea, under the Global Research Support Program in the Digital Field program (0420-20250022) supervised by the IITP(Institute for Information & Communications Technology Planning & Evaluation)

References

[1] ITER Physics Basis Editors *et al*. 1999 Nucl. Fusion **39** 2137.

[2] P.C. de Vries *et al.* 2011 Nucl. Fusion **51** 053018.

[3] G. Marceca *et al.* 2020 NeurIPS **11**.

[4] G. Shin *et al.* 2020 Fusion Eng. Des. **157** 111634.

[5] F. Matos *et al.* 2020 Nucl. Fusion **60** 036022.

[6] M. Zorek *et al.* 2022 Plasma Phys. Controlled Fusion **64** 125004.

[7] F. Matos *et al.* 2021 Nucl. Fusion **61** 046019.

[8] B. Kim *et al.* 2024 Rev. Sci. Instrum. **95** 104701.

[9] K. Gill *et al.* 2024 Mach. Learn.: Sci. Technol. **5** 035012.

[10] W. Biel *et al.* 2019 Fusion Eng. Des. **146** 465-472.

[11] G.S. Lee *et al.* 2000 Nucl. Fusion **40** 575-582.

[12] L. McInnes *et al.* 2020 arXiv:1802.03426.

[13] S. Liu *et al.* 2018 CVPR 8759-8768.